The Journal of Headache and Pain

RESEARCH

Open Access

Regional distribution of unbound eletriptan and sumatriptan in the CNS and PNS in rats: implications for a potential central action

Nana Svane[1], Frida Bällgren[2], Aghavni Ginosyan[2], Mie Kristensen[1], Birger Brodin[1*†] and Irena Loryan[2*†]

Abstract

Background Triptans are potent 5-$HT_{1B/1D/1F}$ receptor agonists used in migraine therapy, thought to act through peripheral mechanisms. It remains unclear whether triptans cross the blood-brain barrier (BBB) sufficiently to stimulate central 5-$HT_{1B/1D/1F}$ receptors. This study investigates the disposition of eletriptan and sumatriptan in central nervous system (CNS) and peripheral nervous system (PNS) regions and predicts regional 5-$HT_{1B/1D/1F}$ receptor occupancies at clinically relevant concentrations.

Methods Using the Combinatory Mapping Approach (CMA) for regions of interest (ROI), we assessed the unbound tissue-to-plasma concentration ratio ($K_{p,\,uu,\,ROI}$) in rats at steady state across CNS (hypothalamus, brain stem, cerebellum, frontal cortex, parietal cortex, striatum, hippocampus, whole brain, and spinal cord) and PNS (trigeminal ganglion and sciatic nerve) regions. We used $K_{p,\,uu,\,ROI}$ values to estimate unbound target-site concentrations and 5-$HT_{1B/1D/1F}$ receptor occupancies in humans.

Results We observed heterogenous triptan transport across CNS and PNS regions with the highest extent of unbound drug transport across the blood-nerve barrier in the trigeminal ganglion ($K_{p,\,uu,\,TG}$: eletriptan: 0.519, and sumatriptan: 0.923). Both drugs displayed restricted entry across the BBB ($K_{p,\,uu,\,whole\ brain}$: eletriptan: 0.058, and sumatriptan: 0.045) combined with high inter-regional variability. We estimated near-complete receptor occupancy in the trigeminal ganglion, while lower occupancies were observed in the whole brain, irrespective of the drug or receptor subtype. For instance, eletriptan was predicted to achieve 84% 5-HT_{1B} receptor occupancy in the trigeminal ganglion and 37% in the whole brain at clinically relevant concentrations.

Conclusions This study suggests that despite low BBB transport, both eletriptan and sumatriptan achieve unbound concentrations sufficient to stimulate 5-$HT_{1B,}$ 5-HT_{1D}, and 5-HT_{1F} receptors not only in the trigeminal ganglion, but also in the CNS. Further research is needed to determine whether central mechanisms contribute to triptan's antimigraine effect and/or side effects.

Keywords Migraine, Eletriptan, Sumatriptan, Blood-brain barrier, CNS, PNS, Central effect, 5-$HT_{1B/1D/1F}$ receptors, Combinatory mapping approach, Free drug theory

†Birger Brodin and Irena Loryan shared corresponding authorship.

*Correspondence:
Birger Brodin
birger.brodin@sund.ku.dk
Irena Loryan
irena.loryan@farmaci.uu.se
Full list of author information is available at the end of the article

Graphical Abstract

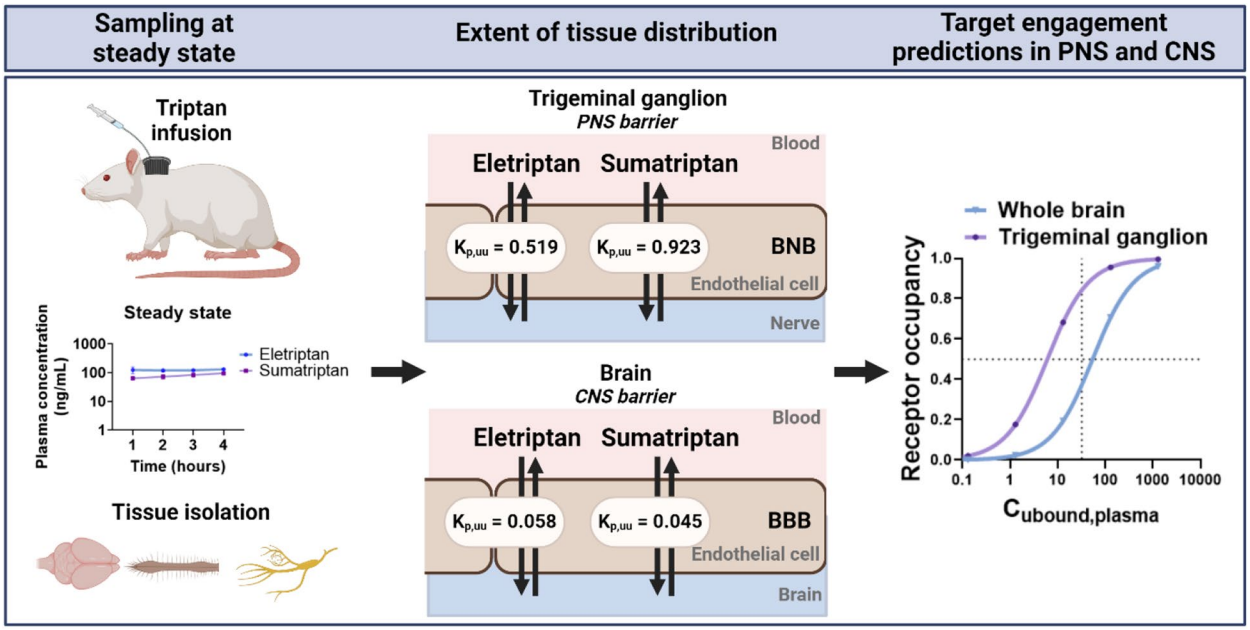

BNB: blood-nerve barrier, BBB: blood-brain barrier, $K_{p,uu}$: unbound tissue-to- plasma concentration ratio

Background

Migraine is a common neurovascular disease affecting approximately 15% of the global population [1, 2]. Triptans are generally considered the most effective class of compounds for the treatment of acute migraine [3]. There are seven triptans in clinical use including sumatriptan, rizatriptan, eletriptan, zolmitriptan, almotriptan, frovatriptan, and naratriptan [4, 5]. Triptans act as potent agonists of the 5-hydroxytryptamine (5-HT) receptor subtype 1B, 1D, and 1F [6]. However, their exact mechanism and site of action remain a subject of ongoing debate [7–9].

Originally, triptans were developed as vasoconstrictors targeting intracranial extracerebral arteries [9, 10]. Nowadays multiple mechanisms have been proposed to account for the antimigraine effect including vascular, trigeminovascular, and central mechanisms, which might act additively (Fig. 1) [10]. The predominant mechanism of action appears to be through trigeminal projections, which is situated in the peripheral nervous system (PNS) [6, 9–11]. Nonetheless, the presence of 5-HT_{1B}, 5-HT_{1D}, and 5-HT_{1F} receptors in various regions of the central nervous system (CNS) highlights that the CNS might also be a potential target area for triptans [12–16].

The PNS is protected by the peripheral blood-nerve barrier (BNB), while the brain is protected by the blood-brain barrier (BBB). The BBB is a highly restrictive barrier that separates the brain parenchyma from the circulatory system as reviewed by Abbott et al. 2010 [17]. In contrast, the BNB is considered less restrictive, as evidenced by higher paracellular transport of 4 kDa dextran and higher extent of the transport of small molecular weight drugs [18].

Triptans are relatively hydrophilic and positively charged at physiological pH. Given their hydrophilic nature and several indications of efflux transporter interactions, triptans are expected to have poor BBB penetrating properties [19–22]. Despite this, there is evidence to suggest that triptans reach the CNS to some extent. For instance, a recent systematic review highlights that triptans may cross the BBB based on diverse neuroimaging studies [23]. Muzzi et al. (2020) further demonstrated rapid brain uptake of sumatriptan in rats, with accumulation in the hypothalamus and brain stem within 1 and 5 min following subcutaneous injections [24]. Additionally, a meta-analysis study of oral triptans have reported CNS-related adverse events such as fatigue, somnolence, and dizziness, which imply CNS involvement [25, 26]. Whether triptans cross the BBB to an extent that significantly contributes to their pharmacological action remains an open question [8, 9, 23, 27, 28].

This study aims to address this question by examining two triptans: the more lipophilic eletriptan and the

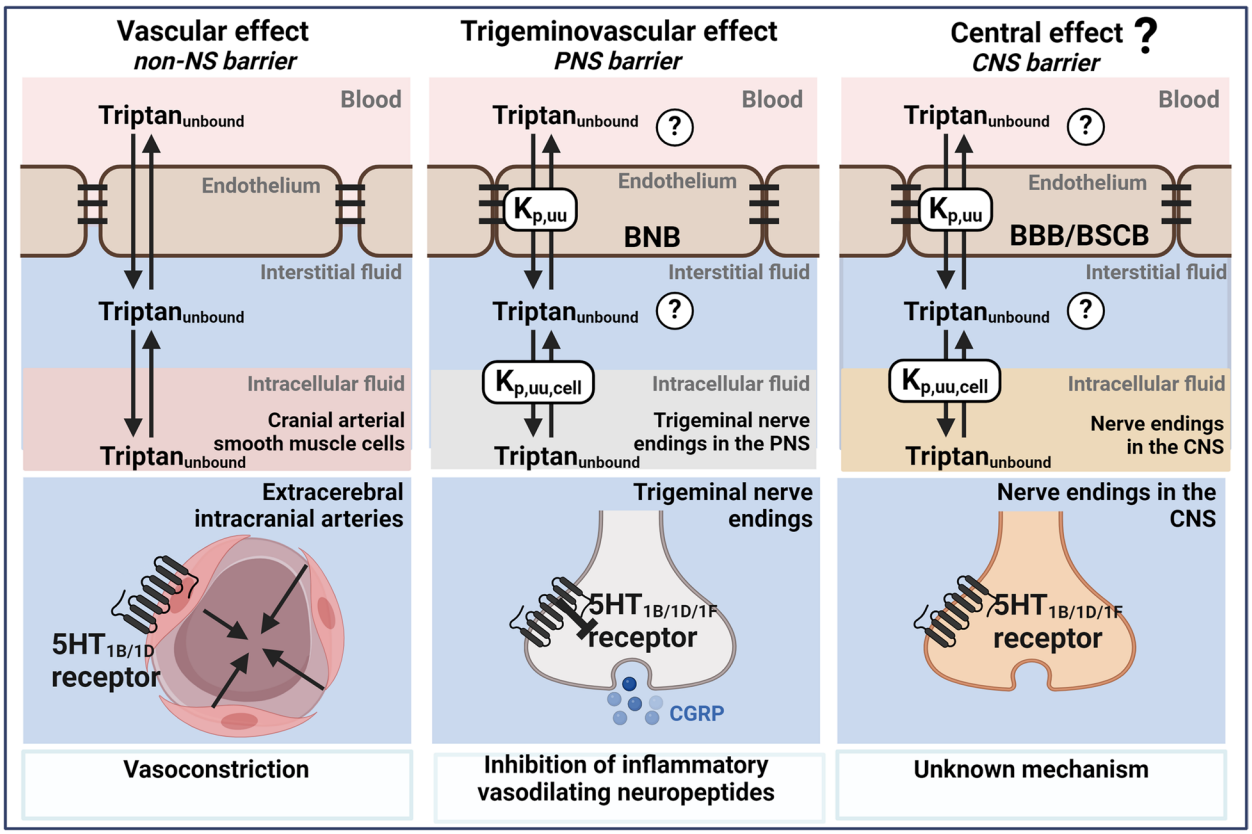

Fig. 1 Schematic illustration of triptan pharmacology from a neuropharmacokinetic point of view. Unbound target-site concentrations are governed by interrelated and interconnected processes including the passage of unbound drug across the blood-to-tissue endothelial interfaces and cellular barriers. Triptans are known to exert their action through 5-$HT_{1B/1D/1F}$ receptors. Their proposed mode of action involves vascular, trigeminovascular, and central mechanisms. For triptans to cause these actions, they need to cross endothelial barriers including the non-nervous system (NS) barriers, PNS barriers (BNB; blood-nerve barrier), and CNS barriers (BBB; blood-brain barrier or BSCB; blood-spinal cord barrier). $K_{p,\,uu}$ is the unbound tissue-to-plasma concentration ratio describing the extent of unbound drug transport across an endothelial barrier and $K_{p,\,uu,\,cell}$ is the unbound intracellular-to-extracellular (interstitial) concentration ratio describing the extent of cellular barrier transport. NB: for simplicity, only key pharmacodynamic mechanisms are illustrated

prototypical more hydrophilic sumatriptan. Specifically, we aim to assess the extent of eletriptan and sumatriptan transport into CNS regions (hypothalamus, brain stem, cerebellum, frontal cortex, parietal cortex, striatum, hippocampus, whole brain, spinal cord) and PNS regions (trigeminal ganglion and sciatic nerve). Additionally, we aim to predict the regional 5-HT_{1B}, 5-HT_{1D}, and 5-HT_{1F} receptor occupancy at clinically relevant triptan concentrations.

Our approach is based on the free-drug theory, which proclaims that only unbound and unionized drug can pass membranes and engage with pharmacological targets [29]. We applied the Combinatory Mapping Approach for Regions of Interest (CMA-ROI), which integrates preclinical neuropharmacokinetic (neuroPK) parameters with information on drug binding in respective matrices measured in vitro using brain slice and equilibrium dialysis assays (Fig. 2) [30, 31]. The CMA-ROI allows the assessment of unbound target-site concentrations for calculations of the unbound tissue-to-plasma concentration ratio ($K_{p,\,uu}$) [30, 31]. In addition, this approach allows the determination of the unbound intracellular-to-brain interstitial concentration ratio ($K_{p,\,uu,\,cell}$) for the characterization of the extent of cellular barrier transport [32, 33].

Here, we determined unbound tissue and plasma concentrations in rats at steady state in order to calculate the $K_{p,uu}$ in various PNS and CNS regions. The highest drug exposure was observed in the trigeminal ganglion revealing $K_{p,\,uu}$ values of 0.519 for eletriptan and 0.923 for sumatriptan. These findings suggest that sumatriptan penetrates the BNB more readily, potentially through passive diffusion or mutually compensated efflux and influx, while eletriptan is subjected to moderate efflux.

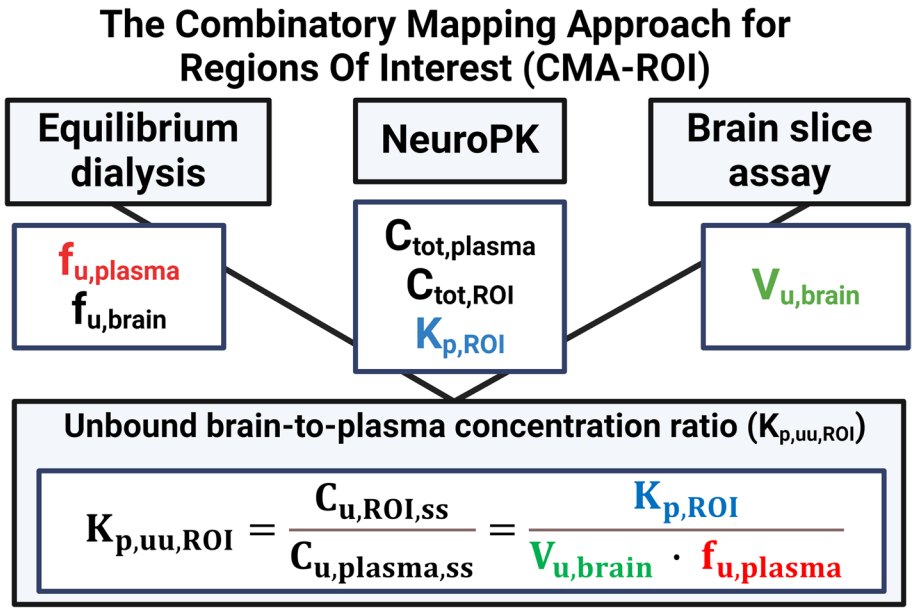

Fig. 2 Schematic illustration of the CMA-ROI. The CMA-ROI combines preclinical neuropharmacokinetic parameters such as $C_{tot,\ plasma}$, $C_{tot,\ ROI}$, and K_p, with in vitro equilibrium dialysis and brain slice techniques to determine drug binding properties in respective matrices ($f_{u,plasma}$, $f_{u,brain}$, $f_{u,nerve}$) and unbound volume of distribution in the brain ($V_{u,\ brain}$). Created with Biorender.com

Both drugs entered the brain parenchyma with $K_{p,\ uu}$ values of 0.058 for eletriptan and 0.045 for sumatriptan, suggesting a low extent of BBB transport due to significant active efflux. Notably, variability in $K_{p,uu}$ was observed across different brain regions. Despite low BBB transport, our predictions suggest that both eletriptan and sumatriptan achieve unbound concentrations sufficient to stimulate 5-$HT_{1B/1D/1F}$ receptors, not only in the trigeminal ganglion, but also in the CNS.

Methods

Chemicals

Sumatriptan succinate (99.94%), sumatriptan-d6 succinate (90%) and eletriptan hydrobromide (98.13%) were ordered from MedChemExpress (New Jersey, USA). Acetonitrile, gradient grade for liquid chromatography, and anhydrous dipotassium hydrogen phosphate were purchased from Merck (Darmstadt, Germany). Formic acid, reagent grade ≥ 95%, sodium chloride (NaCl), potassium chloride (KCl), magnesium sulfate ($MgSO_4$), calcium dichloride ($CaCl_2$), HEPES (N'-2-Hydroxyethylpiperazine-N'-2 ethane sulphonic acid), ascorbic acid, and potassium dihydrogen phosphate (KH_2PO_4) were purchased from Sigma-Aldrich (Steinheim, Germany), and dimethyl sulfoxide (DMSO) was purchased from MP Biomedicals (Eschwege, Germany). The Milli-Q Academic system (Millipore, Bedford, MA, USA; Resistance 18.2 Ohm; Millipak®Express 20 Filter, 0.22 µm) was purchased from Merck Millipore (Burlington, MA, USA).

Animals

Healthy male and female Sprague-Dawley rats weighing 250–325 g (Taconic, Lille Skensved, Denmark) were used for all animal experiments. The selection of male and female rats was based on the intention to have a heterogeneous group of animals. The rats were individually housed by sex, provided with ad libitum access to food and water, and maintained under a 12-hour light-dark cycle at temperatures ranging from 20 to 22 °C and 45–65% humidity. All experiments adhered to the guidelines of the Swedish National Board for Laboratory Animals and were approved by the Animal Ethics Committee of Uppsala, Sweden (Ethical approval number: 5.8.18–12230/2019). The studies were non-blinded and non-randomized. The animal studies have been reported in agreement with the ARRIVE guidelines [34]. A minimally required sample size of four to six animals per group was calculated in order to achieve the desired statistical power for a two-tailed t-test study, given the *p*-value of 0.05, the anticipated effect size, i.e., Cohen's d in the range of 2 to 2.5, and a desired statistical power level of 0.8.

The Combinatory Mapping Approach for regions of interest (CMA-ROI)

The CMA combines in vivo and in vitro experiments to determine the unbound tissue-to-plasma concentration ratio ($K_{p,\ uu}$) [30, 31]. The $K_{p,\ uu}$ value is the state-of-the-art neuropharmacokinetic parameter describing

the extent of drug transport across a barrier [35, 36]. This approach combines: (1) In vivo neuropharmacokinetic studies in rats to determine the plasma and tissue concentrations at steady state to determine the total tissue-to-plasma concentration ratio (K_p), (2) in vitro equilibrium dialysis studies to determine unbound fractions in brain and plasma ($f_{u,\ brain}$ and $f_{u,\ plasma}$), and (3) in vitro brain slice assays to determine the unbound volume of distribution ($V_{u,\ brain}$). In addition, the unbound intracellular-to-extracellular (interstitial) concentration ratio ($K_{p,\ uu,\ cell}$) across brain parenchymal cells can be derived from the CMA. A schematic illustration of the CMA, its methodologies and output parameters are shown in Fig. 2.

In vivo neuropharmacokinetic (neuroPK) study

In vivo neuroPK evaluation of eletriptan and sumatriptan was assessed in rats at steady state with the overall purpose of determining steady state tissue-to-plasma concentration ratios, $K_{p,\ brain}$(Eq. 1). Male ($N=6$) and female ($N=6$) Sprague-Dawley rats were used for neuroPK experiments. Surgical implantation of catheters in the femoral vein and femoral artery for intravenous (IV) drug infusion and arterial blood sampling was done one day prior to the experiments. During the procedure, the animals were placed on a heating pad under anesthesia induced by 5% isoflurane and maintained by 2.5% isoflurane, supplemented with 3 L/min oxygen. After catheterization, the rats were individually transferred to a CMA120 system (CMA, Solna, Sweden). On the day of the experiment, awake rats were weighed, and the loading and maintenance doses were calculated based on individual weights (Table 1). The rats were initially given a 10-minute fast-rate IV loading dose followed by a constant 4-hour infusion. The dosing regimen was chosen based on publicly available pharmacokinetic parameters in rats (volume of distribution and clearance) to achieve a steady state plasma concentration corresponding to clinically relevant concentrations of 150–200 ng/mL [37, 38].

Blood samples were collected from the vein catheter before (0 h) and at 1, 2, 3, and 4 h after the start of the drug infusion and terminally by heart puncture. Plasma was isolated from the blood samples by centrifugation at 10,000 rpm for 5 min. After decapitation, the brain was isolated and dissected into two halves. One half was microdissected with isolation of regions of interest such as the frontal cortex, parietal cortex, cerebellum, hippocampus, hypothalamus, brain stem, and striatum. The second half was also collected and referred to as the whole brain. The spinal cord, sciatic nerve, and trigeminal ganglion were also sampled. The sciatic nerve was included as a comparable peripheral nerve tissue to the trigeminal ganglion due to its distinct anatomical location and ease of isolation. The dissected tissues were cleaned by removing large blood vessels. All samples were transferred to ceramic microbead-containing vials (VWR, Sweden), weighed, and immediately placed at -80 °C. Before analysis, tissue samples were mixed with 1:4 (w: v) phosphate-buffered saline pH 7.4 (PBS) and homogenized mechanically on a Mini Bead Mill (VWR, Sweden). Samples were immediately frozen and stored at -80 °C.

Table 1 A summary of used steady state intravenous infusion regimen for in vivo neuropharmacokinetic studies

Drug	Loading dose (µg/kg/min)	Maintenance dose (µg/kg/min)	Total dose (mg/kg)
Eletriptan	218	22	7.5
Sumatriptan	49	6.8	2.1

The $K_{p,\ ROI}$ was calculated as:

$$K_{p,ROI} = \frac{C_{tot,ROI,ss}}{C_{tot,plasma,ss}} \quad (1)$$

Where $C_{tot,ROI,ss}$ is the total concentration of a drug in tissue at steady state corrected for a residual drug in blood according to Fridén et al. [39], $C_{tot,plasma,ss}$ is the total concentration of a drug in plasma at steady state.

Small volumes of contaminating blood may contribute to the overestimation of drug concentrations in tissue, particularly when investigating low BBB permeable drugs, where blood concentrations are significantly higher than brain concentrations. Hence, the total drug concentration in tissue corrected for residual blood was calculated as:

$$C_{tot,ROI,ss} = \frac{C_{tot,ROI,ss,uncorrected} - V_{eff}.C_{tot,plasma,ss}}{1 - V_{water}} \quad (2)$$

Where V_{water} is the apparent brain vascular volume of plasma water (10.3 µL/g brain), and V_{eff} is the effective plasma volume. V_{eff} was calculated as [39]:

$$V_{eff} = f_{u,plasma} \cdot V_{water} + \left(1 - f_{u,plasma}\right) \cdot V_{protein} \quad (3)$$

Where $f_{u,\ plasma}$ is the fraction of unbound drug in plasma, $V_{protein}$ is the apparent brain vascular volume of plasma protein (7.99 µL/g brain) [39].

Equilibrium dialysis

Assessment of the unbound fraction of eletriptan and sumatriptan in plasma ($f_{u,plasma}$), brain ($f_{u,brain}$), and

sciatic nerve ($f_{u,nerve}$) were performed by equilibrium dialysis using an HTD 96b equilibrium dialysis device (HTDialysis, CT, USA) [40]. This method takes advantage of the ability of unbound drug being able to penetrate a semipermeable membrane, while protein-bound drug cannot. The semipermeable membrane separates a protein-containing compartment from a protein-free buffer compartment allowing estimation of the extent of drug tissue binding properties at equilibrium. A schematic illustration of the equilibrium dialysis principle is shown in Fig. 4A. Equilibrium dialysis experiments were performed using three biological and three technical replicates unless otherwise stated. The two chambers of the equilibrium dialysis wells were separated by a semipermeable cellulose membrane with a cutoff of 12–14 kDa. The cellulose membrane was prepared according to the manufacturer's recommendations (HTDialysis, CT, USA). Tissues were homogenized mechanically using microbead-containing vials on a Mini Bead Mill (VWR, Sweden) followed by further short homogenization using a Vibra Cell ultrasonic processor VCX-130 (Chemical instruments A/B, Sweden). The final concentration of eletriptan and sumatriptan was 1 µM in tissue homogenate, and 200 or 400 nM in plasma. The rationale for selecting a concentration of 1 µM in tissue homogenate was to ensure the quantification of highly bound drugs. Two concentrations were evaluated in plasma, matching expected plasma concentrations in neuroPK studies which were relatively compatible with clinically relevant human peak plasma concentrations [37, 38].

One chamber was filled with 100 µL of PBS. The second chamber was filled with 100 µL of a drug containing undiluted plasma or tissue homogenate 1:9 (w: v) brain or sciatic nerve homogenate in PBS. The dialysis was running for 6 h on orbital shaker at 37 °C, 200 rpm. After 6 h, 50 µL samples were taken from the buffer and plasma/tissue compartments. Buffer samples were added to an equal amount of plasma/tissue, while plasma/tissue samples were added to an equal amount of buffer to match the matrices required for bioanalysis. Samples were immediately frozen and stored at -80 °C.

Thermostability and recovery of the compounds were controlled in plasma or brain homogenate in parallel with the experiment. Samples were taken before and after the 6-hour incubation at 37 °C, 200 rpm. A thermostability of 100 ± 30% of the initial drug concentration was accepted. The thermostability was calculated as:

$$\text{Termostability (\%)} = \frac{C_{6\text{ hours}}}{C_{0\text{ hours}}} \cdot 100\% \quad (4)$$

Where $C_{0\text{ hours}}$ and $C_{6\text{ hours}}$ are the concentrations in plasma/brain homogenate before and after incubation.

The recovery of the spiked drug concentration into the plasma/brain homogenate was calculated in percentage of theoretical drug concentrations to evaluate potential sticking to the plastic. The recovery was calculated as:

$$\text{Recovery (\%)} \frac{C_{0\text{ hours}}}{C_{\text{theoretical}}} \cdot 100\% \quad (5)$$

Where $C_{theoretical}$ is the actual spiked buffer concentration.

The unbound fraction of drug in plasma ($f_{u,plasma}$) was calculated as:

$$f_{u,plasma} = \frac{C_{buffer}}{C_{plasma}} \quad (6)$$

Where C_{buffer} represents the drug concentration in the buffer/receiver compartment and C_{plasma} represents the drug concentration in the plasma/donor compartment at the end of 6-hour incubation.

The unbound fraction of drug in diluted brain homogenate ($f_{u,D,brain}$) was calculated as:

$$f_{u,D,brain} = \frac{C_{buffer}}{C_{brain}} \quad (7)$$

Where C_{brain} represents the drug concentration in the diluted brain homogenate/donor compartment.

To account for the dilution of brain homogenate, the unbound fraction of drug in undiluted brain homogenate ($f_{u,\,brain}$) was calculated as:

$$f_{u,brain} = \frac{\frac{1}{D}}{\left(\frac{1}{f_{u,D,brain}} - 1\right) + \frac{1}{D}} \quad (8)$$

Where D represents the dilution factor of the homogenate in PBS and is equal to 10 in this experiment.

In vitro brain slice assay

Assessment of the intracellular distribution of unbound eletriptan and sumatriptan was performed by the in vitro brain slice method [41, 42]. A schematic illustration of the brain slice principle is shown in Fig. 4D. Artificial extracerebral fluid (aECF) was prepared using ultra-pure water (Millipore, MA, USA) supplemented with 129 mM NaCl, 3 mM KCl, 1.2 mM $MgSO_4$, 25 mM HEPES, K_2HPO_4, 1.4 mM $CaCl_2$, 0.4 mM ascorbic acid, and 10 mM glucose, and adjusted to pH 7.3 at 37 °C. The aECF was equilibrated with 100% oxygen for 15 min. The brain

was isolated from naïve male rats ($N=3$ per drug). Coronal slices of the brain were performed using a vibrating blade microtome (Leica Microsystems AB, Sweden) with a slice thickness of 300 µm. Six slices were transferred to a beaker with ice-cold aECF for approximately 5 min. The brain slices were transferred to a beaker with 15 mL of prewarmed aECF containing 100 nM eletriptan or sumatriptan and sealed with a breathable film (Diversified Biotech MA, USA). The brain slices in aECF were transferred to a benchtop orbital shaker (MaxQ4450, Thermo Scientific, MA, USA) and incubated for 5 h at 37 °C, 45 rpm, and 75–80 mL O_2/min. The pH of the aECF containing brain slices was between 7.2 and 7.4 after 5-hour incubation. The aECF buffer was sampled from the brain slice containing beaker after the achievement of equilibrium at 5 h (C_{buffer}). All aECF samples were mixed 1:1 (v: v) with 1:4 (w: v) brain homogenate in aECF. Brain slices were dried on filter paper, individually weighed, and homogenized with 1:9 (w: v) of aECF using a Vibra Cell ultrasonic processor VCX-130 (Chemical instruments A/B, Sweden) for 5 s at 50% amplitude. Samples were immediately frozen and stored at -20 °C.

The thermostability of the compounds was assessed in parallel with the experiment. Samples were taken from a solution without brain slices before and after the 5-hour incubation at 37 °C, 45 rpm. A thermostability of 100 ± 30% of the initial drug concentration was accepted.

$$\text{Termostability } (\%) = \frac{C_{5\text{ hours}}}{C_{0\text{ hours}}} \cdot 100\% \tag{9}$$

Where $C_{0\text{ hours}}$ and $C_{5\text{ hours}}$ are the concentrations in buffers before and after incubation. The recovery of the spiked drug concentration into the buffer solution was calculated according to Eq. 5.

Assuming that the drug concentration in the protein free aECF corresponds to the concentration in the brain interstitial fluid (ISF) at equilibrium, the $V_{u,\text{ brain}}$ was calculated as:

$$V_{u,brain} = \frac{A_{brain}}{C_{u,brain\ ISF}} \approx \frac{A_{brain}}{C_{buffer}} => \frac{A_{brain} - V_i \cdot C_{buffer}}{C_{buffer} \cdot (1 - V_i)} \tag{10}$$

Where A_{brain} represents the drug amount per g brain in the brain slice, C_{buffer} represents the dug concentration in aECF, V_i represents the leftover volume of the buffer on the brain slice and has previously been determined to 0.133 mL/g brain [18].

NeuroPK parameters

Determined parameters from in vivo and in vitro studies were applied to determine key neuroPK parameters. The unbound tissue-to-plasma concentration ratio ($K_{p,uu}$) was calculated as:

$$K_{p,uu,tissue} = \frac{K_{p,tissue}}{V_{u,brain} \cdot f_{u,plasma}} \tag{11}$$

The observed unbound intracellular-to-interstitial concentration ratio ($K_{p,uu,cell,obs}$) can be estimated based on $f_{u,brain}$ and $V_{u,brain}$ [32]. A schematic illustration of the brain slice principle is shown in Fig. 4F The $K_{p,uu,cell}$ was calculated as:

$$K_{p,uu,cell,obs} = \frac{C_{u,ICF,ss}}{C_{u,ISF,ss}} = V_{u,brain} \cdot f_{u,brain} \tag{12}$$

Where $C_{u,ICF}$ is the unbound concentration in the intracellular fluid (ICF) and $C_{u,ISF}$ is the unbound concentration in the ISF [34].

The unbound cell partitioning ratio can be predicted ($K_{p,uu,cell,pred}$) based on the assumption that only unbound and unionized drug can pass through the cellular membrane by passive diffusion mechanism [33]. Using physiological volumes and pH of ISF, cytosol and lysosomes as well as predicted pK_a values of drugs, the $K_{p,uu,cell,pred}$ can be predicted as:

$$K_{p,uu,cell,pred} = V_{ISF} + K_{p,uu,cyto,pred} \cdot \left(V_{cyto} + V_{lyso} \cdot K_{p,uu,lyso,pred}\right) \tag{13}$$

Where V_{ISF} is 0.2 mL/g brain, V_{cyto} is 0.79 mL/g brain, and V_{lyso} is 0.01 mL/g brain [33].

The $K_{p,\text{ uu, cytosol, pred}}$ can be calculated as:

$$K_{p,uu,cyto,pred} = \frac{10^{\left(pKa - pH_{cyto}\right)} + 1}{10^{(pka - pH_{ISF})} + 1} \tag{14}$$

Where $pH_{cytosol}$ is 7.02, pH_{ISF} is 7.3 [33], predicted $pKa_{eletriptan}$ is 8.4, and predicted $pKa_{sumatriptan}$ is 9.5 [43].

The $K_{p,\text{ uu, lyso, pred}}$ of basic drugs can be calculated as:

$$K_{p,uu,lyso,pred} = \frac{10^{\left(pKa - pH_{lyso}\right)} + 1}{10^{\left(pka - pH_{cyto}\right)} + 1} \tag{15}$$

Where pH_{lyso} is 5.18 [33].

Sample preparation and bioanalysis

Quantification of sumatriptan and eletriptan in plasma and tissues was conducted using ultra-performance liquid chromatography coupled with tandem mass spectrometry (UPLC-MS/MS). The method for the

assessment of plasma and tissue concentrations was developed based on previously published protocols with modifications [22, 44–52]. Total sumatriptan and eletriptan in plasma and tissue samples were quantified using Acquity UPLC coupled with Xevo TQ-S Micro triple quadrupole mass spectrometer (MS/MS) (Waters Corporation, Milford, MA, USA). The bioanalytical method parameters and sample preparation details are described in Additional file 1. Acceptance criteria were predefined according to the FDA guidance [53]. Sumatriptan, eletriptan and internal standard sumatriptan-d6 were analyzed in positive electrospray ionization mode with multiple reaction monitoring (MRM) mode to monitor Parent → Product ion (m/z) transitions, respectively. Preparation of plasma and tissue samples, respective standards, quality control samples, and blanks, plasma, and tissue homogenates, were conducted in two steps. Plasma and tissue homogenate samples, with respective blanks, standards and quality controls were precipitated in acetonitrile 1:3 (v: v) with internal standard (sumatriptan-d6) followed by centrifugation. The supernatant was diluted 1:2 (v: v) in the mobile phase (MP) A, i.e., 0.1% formic acid in ultra-pure water.

The chromatographic separation of analytes was conducted using ACQUITY UPLC HSS C18 column, 2.1 × 100 mm, 1.8 µm, protected by an ACQUITY UPLC BEH C18 VanGuard pre-column, 2.1 × 5 mm, 1.7 µm (Waters Corporation, Milford, MA, USA) at 30 °C with a flow rate of 0.3 mL/min. MPA; 0.1% formic acid, and MPB; 0.1% formic acid in acetonitrile, were employed in gradient for separation of analytes and their elution. Details on mobile phase gradient can be found in Additional file 1.

The linear range with a determination coefficient equal to or higher than 0.99 was obtained in all standard curves prepared in the respective control matrices using the cassette approach, i.e., including sumatriptan and eletriptan at each standard level. The concentration range in the standard curves was 0.5–220 ng/mL for both sumatriptan and eletriptan (10 levels) in plasma and blank brain homogenate solution, and five levels of quality control samples for both matrices were prepared with concentrations of sumatriptan and eletriptan of 0.8 ng/mL, 4.0 ng/mL, 40 ng/mL, 80 ng/mL, 120 ng/mL, respectively. A 2-1000 nM (8 levels) range was employed for the equilibrium dialysis and brain slice assay experiments. The lowest standard points were set as limits of quantification. Data quantification was done using Masslynx v4.2 (Waters Corporation, Milford, MA, USA).

Prediction of receptor occupancy based on neuropharmacokinetic data

Prediction of receptor occupancies (RO) was based on rat $K_{p,uu}$ values and publicly available equilibrium dissociation constants (K_d) and was assessed according to Hill's equation:

$$RO_{ROI} = \frac{C_{u,ROI^n}}{C_{u,ROI^n} + K_d} \quad (16)$$

Where $C_{u,\,ROI}$ is the unbound concentration of a drug at ROI since only unbound drug is available for target engagement, *n* is Hill's coefficient, which was set to 1.0, supported by reported values [54]. In the present study, i*n vitro* K_d and K_i values for human 5-$HT_{1B/1D}$ and 5-HT_{1F} receptors, respectively were obtained from Napier et al. [55].

Unbound target-site concentrations ($C_{u,ROI}$) in humans were as follows:

$$C_{u,ROI} = C_{tot,plasma} \cdot f_{u,plasma} \cdot K_{p,uu,ROI} \quad (17)$$

Where $C_{tot,plasma}$ is the plasma concentration in humans selected based on publicly available data, $f_{u,\,plasma}$ is the fraction of unbound drug in plasma in humans (Table 2), and $K_{p,uu,ROI}$ is unbound brain-to-plasma concentration ratio assessed in rats.

Statistical analysis

Statistical analysis and figure formatting were performed using GraphPad Prism 10.2.0 (CA, USA). Data are presented as mean ± standard deviation (SD). n denotes biological replicates; N denotes technical replicates. Normality test performance of each dataset was performed by a Shapiro-Wilk test. If stated, groups were compared using two-tailed unpaired student's t-test or by a two-way ANOVA analysis followed by a Tukey's multiple comparison test. *P*-values < 0.05 were considered statistically significant where *: $p \leq 0.05$. **: $p \leq 0.01$. ***: $p \leq 0.001$. ****: $p \leq 0.0001$.

Results

Heterogeneous transport across PNS and CNS barriers with the highest triptan exposure in the PNS

We assessed the total drug concentrations of eletriptan and sumatriptan in CNS regions, PNS regions, and in plasma under steady state as shown in Fig. 3A. Eletriptan and sumatriptan achieved steady state plasma concentrations after a 4-hour dosing regimen (Additional file 2 A) reaching targeted mean $C_{tot,\,plasma}$ of 123 ± 14 and 106 ± 39 ng/mL, respectively (Additional file 2B). The 4-hour

Table 2 Prediction of 5-HT_{1B}, 5-HT_{1D}, and 5-HT_{1F} receptor occupancy levels in the PNS and CNS. The trigeminal ganglion (TG) represents the PNS region, while whole brain (WB) represents the CNS region. Predictions are based on unbound maximal target site concentrations after therapeutic doses of eletriptan and sumatriptan in humans

Parameter	Unit	Site	Eletriptan	Sumatriptan	
			PO 40 mg	PO 50 mg	PO 100 mg
$K_{d,5-HT1B}$ [51]	nM	NA	3.14	11.07	
$K_{d,5-HT1D}$ [51]	nM	NA	0.92	6.58	
$K_{i,5-HT1F}$ [51]	nM	NA	10.23	13.18	
$f_{u,\ plasma}$ [50]			0.13	0.66	
$C_{tot,\ max}$ [35, 36]	nM or (*ng/mL*)	Plasma	246 (*94.0*)	102 (*30.1*)	180 (*53.2*)
$C_{u,\ max}$	nM or (*ng/mL*)	Plasma	32.2 (*12.3*)	67.3 (*19.9*)	119 (*35.1*)
$C_{u,\ max,\ ROI}$	nM	TG	16.6	62.1	109.8
$C_{u,\ max,\ ROI}$	nM	WB	1.86	3.00	5.31
RO_{5-HT1B}	%	TG	84	85	90
RO_{5-HT1B}	%	WB	37	21	32
RO_{5-HT1D}	%	TG	95	90	94
RO_{5-HT1D}	%	WB	67	31	45
RO_{5-HT1F}	%	TG	62	82	89
RO_{5-HT1F}	%	WB	15	19	29

PO peroral, *TG* trigeminal ganglion, *WB* whole brain, *RO* receptor occupancy. The $C_{u,max,ROI}$ has been calculated according to Eq. 17. The RO has been calculated according to Eq. 16. *NA* not applicable

infusion regimen differs from typical clinical practice. However, it was implemented to ensure achievement of steady state concentrations essential for the calculation of K_p and $K_{p,\ uu}$.

Eletriptan demonstrated $K_{p,\ ROI}$ values ranging from 0.107 to 2.960, with the highest values observed in the trigeminal ganglion followed by the sciatic nerve, hypothalamus, hippocampus, striatum, whole brain, spinal cord, cerebellum, brain stem, frontal cortex, and parietal cortex. Sumatriptan showed $K_{p,\ ROI}$ values ranging from 0.021 to 1.582, with the highest values observed in the trigeminal ganglion followed by the sciatic nerve, spinal cord, hypothalamus, whole brain, cerebellum, brain stem, hippocampus, frontal cortex, parietal cortex, and striatum. Eletriptan exhibited higher K_p values than sumatriptan across all investigated regions (Fig. 3B). By exclusively considering the partitioning of unbound drug ($K_{p,uu}$), we noted a similar distribution between the two triptans (Fig. 3C). Eletriptan demonstrated $K_{p,uu,ROI}$ values ranging from 0.019 to 0.519, while sumatriptan demonstrated $K_{p,\ uu,\ ROI}$ values ranging from 0.008 to 0.923. Both drugs showed limited entry into the brain ISF, with $K_{p,uu,whole\ brain}$ values of 0.058 for eletriptan and 0.045 for sumatriptan. Among the brain regions, we found a 7.5-fold difference in $K_{p,\ uu}$ for eletriptan ranging from the lowest in the parietal cortex to the highest in hypothalamus. For sumatriptan, we found a 6.4-fold inter-brain regional difference in $K_{p,\ uu}$ ranging from the lowest in the striatum and the highest in hypothalamus.

Overall, these findings show that eletriptan and sumatriptan are profoundly influenced by the type of endothelial barrier, with increased drug exposure observed in tissues protected by the BNB compared to those protected by the BBB.

Eletriptan and sumatriptan displayed differences in tissue binding and unbound volume of distribution in the brain but similar cellular partitioning

Unbound fractions of eletriptan and sumatriptan in plasma ($f_{u,plasma}$) and in brain homogenate ($f_{u,brain}$) were determined using equilibrium dialysis. We found moderate plasma protein binding of eletriptan and sumatriptan as indicated by mean $f_{u,plasma}$ of 0.31 and 0.67, respectively. These values were obtained using clinically relevant plasma concentrations of 200 nM, matching the concentrations achieved in the neuroPK studies (Fig. 4B). At a higher concentration of 400 nM, the $f_{u,plasma}$ of eletriptan remained unchanged, while a 1.3-fold increase ($p < 0.01$) was found for sumatriptan (Additional File 4). In the brain, eletriptan revealed a $f_{u,\ brain}$ of 0.14, while sumatriptan remained completely unbound with a $f_{u,\ brain}$ approaching 1.0 (Fig. 4C). To ensure uniform non-specific binding across tissues, we assessed the binding properties of eletriptan and sumatriptan in nerve and brain tissue, finding no significant differences (Additional file 5). This supports the use of brain homogenate binding as a surrogate for nerve tissue binding for these compounds, consistent with previous studies [18, 56].

The $V_{u,brain}$ was assessed using brain slice assays. This parameter accounts for both brain tissue binding and intracellular uptake allowing transmembrane pH gradients across intact cell membranes. A schematic illustration of the brain slice principle is shown in Fig. 4D. Eletriptan exhibited significantly higher distribution into brain tissue as compared to sumatriptan, with mean $V_{u,brain}$ of 18.4 mL/g brain and 2.6 mL/g brain, respectively (Fig. 4E).

We estimated the intracellular-to-extracellular cell partitioning coefficients ($K_{p,uu,cell}$), derived from $f_{u,brain}$ and $V_{u,brain}$ according to Eq. 12 [32, 33]. $K_{p,uu,cell}$ describes the extent of transport across cellular membranes, reflecting the involvement of active transport processes (Fig. 4F). Despite significant differences in non-specific binding and unbound volume of distribution in the brain, eletriptan and sumatriptan showed similar $K_{p,uu,cell}$ values

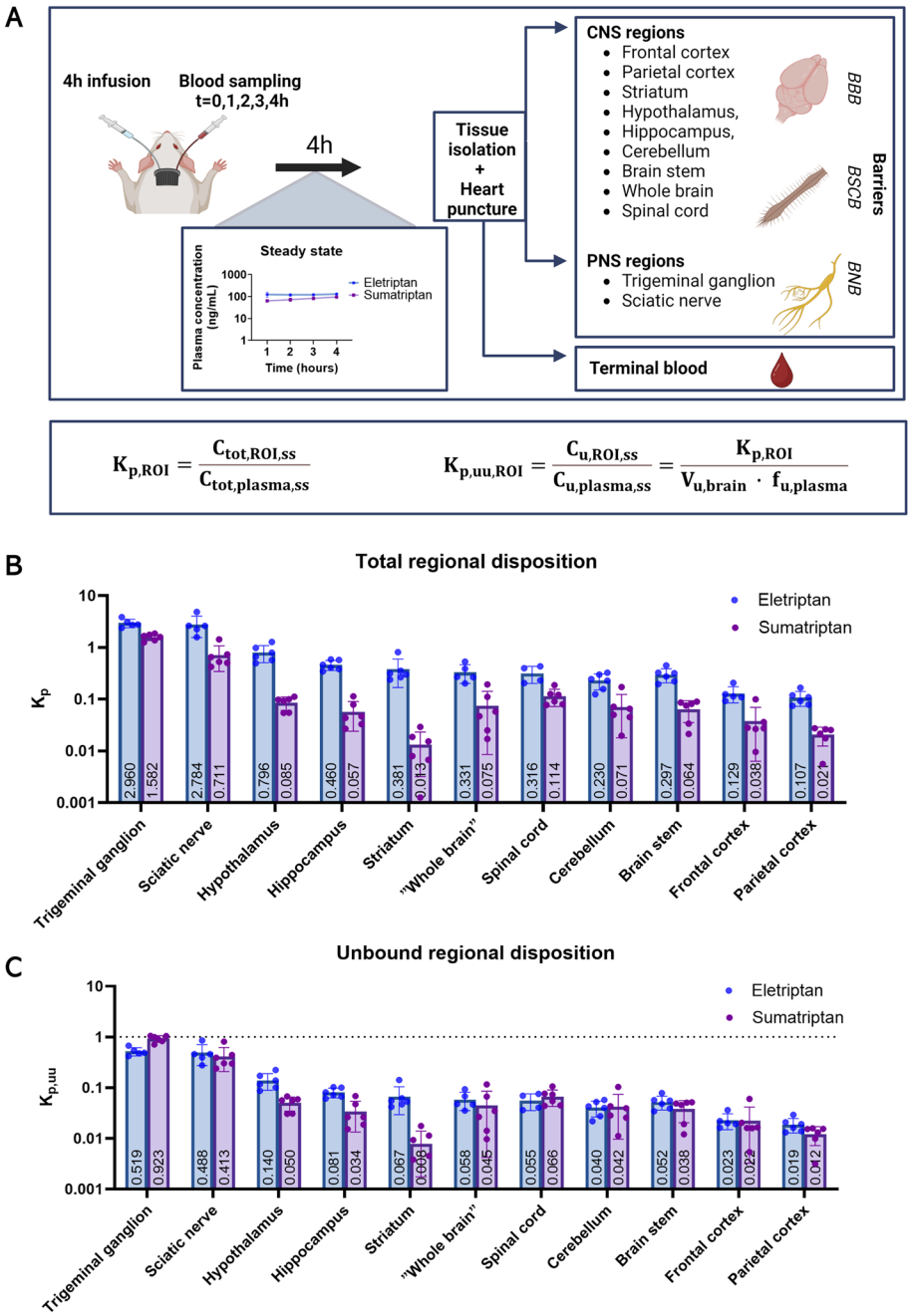

Fig. 3 Assessment of regional K_p and $K_{p,uu}$ for eletriptan and sumatriptan in rats under steady state. **A** Schematic overview of the neuropharmacokinetic study. Male and female rats were given a 4-hour IV infusion of eletriptan or sumatriptan to achieve steady state conditions. After 4 h, blood samples were collected terminally by heart puncture and tissues of interest were isolated including CNS regions: spinal cord, hypothalamus, striatum, cerebellum, brain stem, frontal cortex, and parietal cortex as well as whole brain, and PNS regions: trigeminal ganglion and sciatic nerve. Created with Biorender.com. **B** Total tissue-to-plasma concentration ratio (K_p). **C** The unbound tissue-to-plasma concentration ratio ($K_{p,uu}$). Columns represent mean ± SD (n = 4–6). The mean value of each column is annotated within each bar. The dotted line represents the line of unity. Values below unity indicate predominant active efflux across the respective barriers. In Fig. 3B and C, regions are sorted according to descending $K_p/K_{p,uu}$ values for eletriptan. NB: in B and C a semilogarithmic scale is used for the visualization of data. Data are presented with a linear scale in Additional File 3

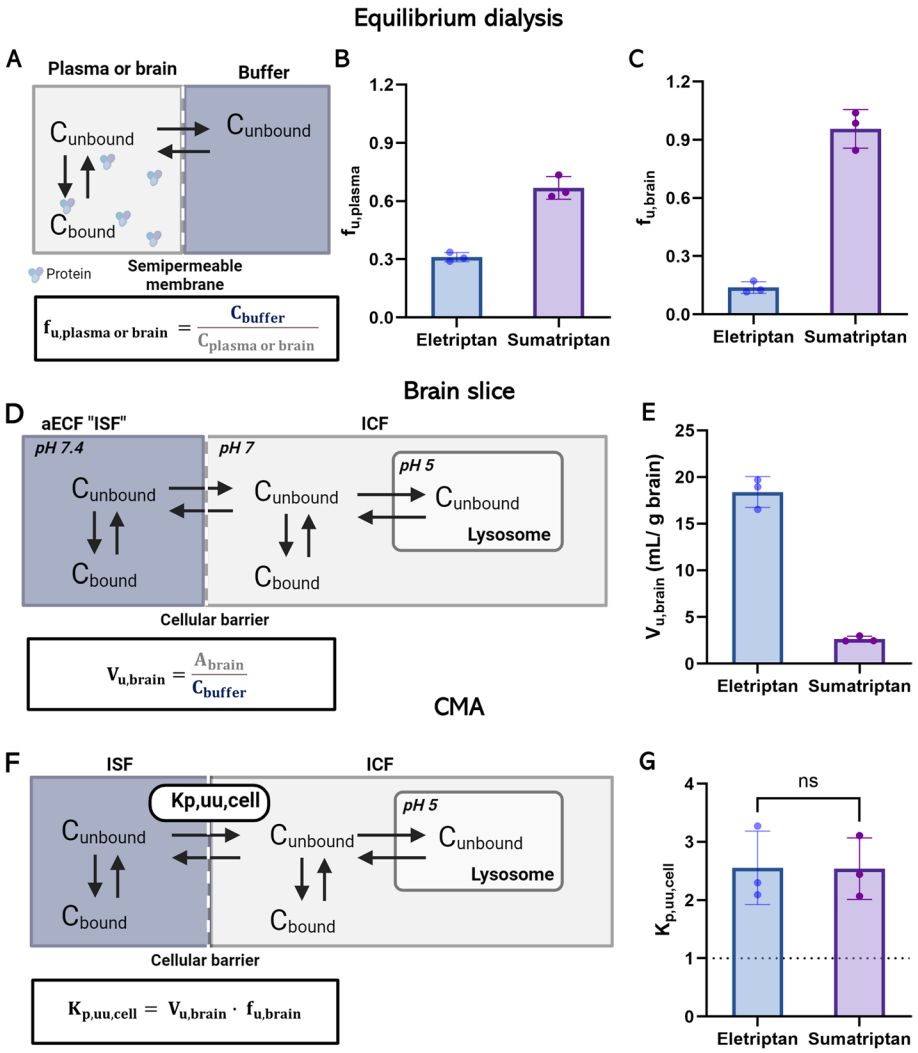

Fig. 4 Plasma and brain tissue binding, unbound volume of distribution, and cellular partitioning in rat tissue. **A** Schematic illustration of the principle behind equilibrium dialysis. Only unbound drug ($C_{unbound}$) can penetrate the semipermeable membrane allowing estimation of the extent of drug tissue binding at equilibrium. **B** The $f_{u,plasma}$ of eletriptan and sumatriptan assessed at 200 nM ($n=3$, $N=3$). **C** The $f_{u,\ brain}$ eletriptan and sumatriptan in brain homogenate assessed at 1 µM ($n=3$, $N=3$). **D** Schematic illustration of the principle behind $V_{u,brain}$. The distribution of unbound drug from artificial extracellular fluid (aECF), which mimics brain ISF, into the ICF of brain parenchymal cells allows for transmembrane pH gradients, also enabling lysosomal trapping. **E** The $V_{u,brain}$ of eletriptan and sumatriptan (100 nM) in rat brain slices ($n=3$, $N=5$). **F** Schematic illustration of the principle behind $K_{p,\ uu,\ cell}$. **G** Estimated $K_{p,\ uu,\ cell}$ of eletriptan and sumatriptan at equilibrium. In Fig. 4G, the dotted line represents the line of unity. Each column represents mean ± SD. The groups were compared using a student's two-tailed t-test ($n=3$, $N=5$). Created with Biorender.com

of 2.6 and 2.5, respectively. A $K_{p,uu,cell}$ higher than unity indicates intracellular accumulation governed by active uptake or lysosomal trapping in brain parenchymal cells (Fig. 4G). To evaluate whether the observed intracellular accumulation is a result of pH partitioning into the more acidic intracellular and lysosomal environment, we predicted the $K_{p,uu,cell,pred}$ by assuming that only unbound and unionized drug can penetrate cellular membranes via passive diffusion according to Eq. 13 [33]. $K_{p,uu,cell,pred}$ was found to be 2.9 for eletriptan and 3.0 for sumatriptan. The $K_{p,uu,cell,\ pred}$ are in line with the experimental determined $K_{p,uu,cell}$, suggesting that the intracellular accumulation is due to pH partitioning rather than active uptake.

Overall, these findings prove that eletriptan exhibits stronger non-specific binding across the investigated matrices compared to sumatriptan, but similar cell partitioning.

Predicted 5-HT$_{1B/1D/1F}$ receptor occupancies indicate CNS target engagement at clinically relevant triptan concentrations

Prediction of unbound target-site concentrations with linkage to in vitro potencies, is a well-established practice to give indications on in vivo efficacy [57]. In this study, we used the $K_{p,\ uu}$ values of eletriptan and sumatriptan determined herein in rats to estimate the unbound target-site concentrations in humans (Fig. 5A). These estimates were based on reported total maximal plasma concentrations (C_{max}) of eletriptan and sumatriptan in patients [37, 38], adjusted for the $f_{u,\ plasma}$ reported for humans [54].

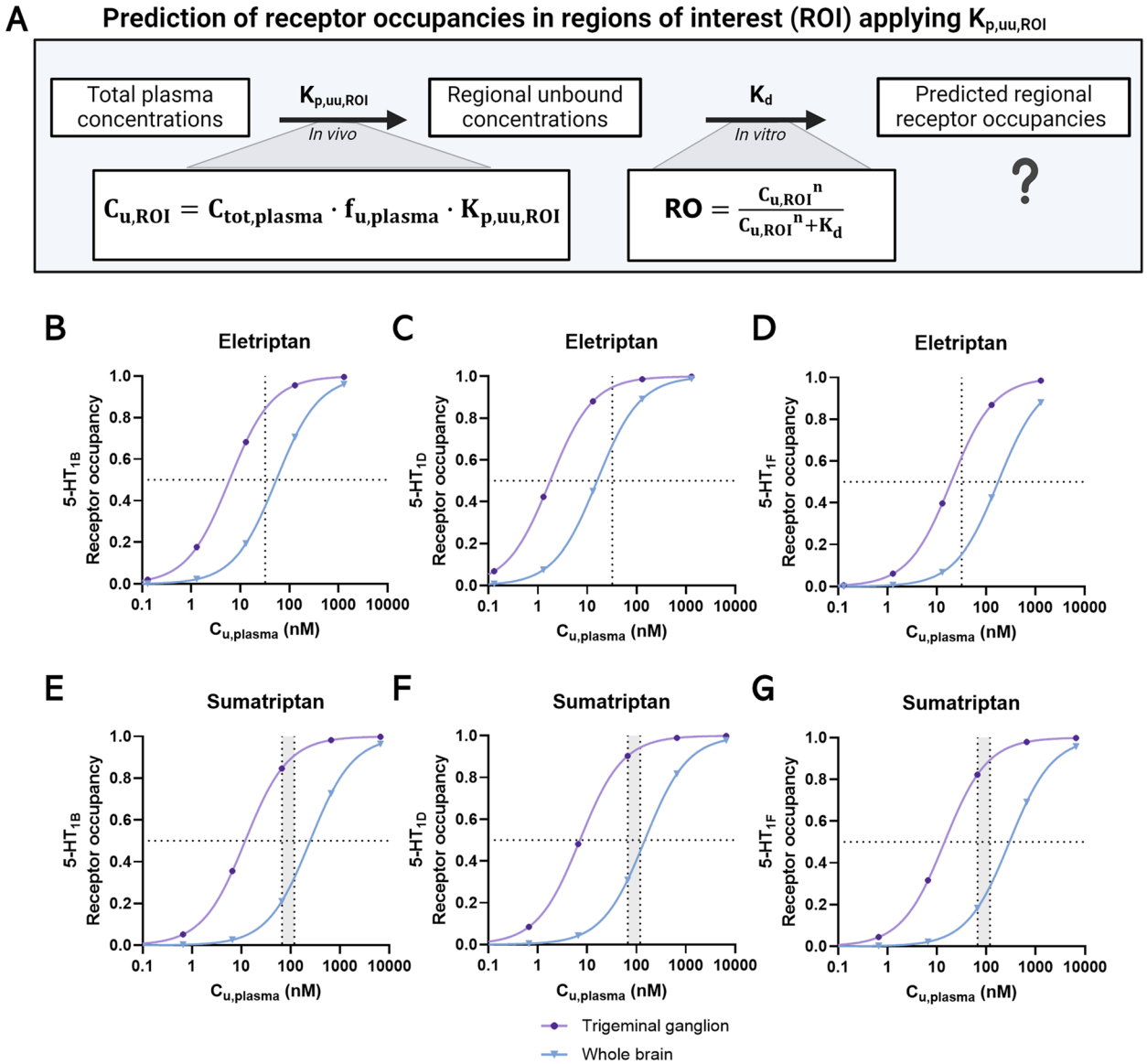

Fig. 5 Predicted 5-HT$_{1B}$,5-HT$_{1D}$, and 5-HT$_{1F}$ receptor occupancies in the trigeminal ganglion and whole brain in humans. **A** Schematic illustration of the principle used to predict unbound target-site concentrations, applying $K_{p,\ uu,\ ROI}$ and in vitro affinity constants to estimate potential target engagement. Created with Biorender.com. Binding dissociation constants, K_d (5-HT$_{1B}$ and 5-HT$_{1D}$) or K_i (5-HT$_{1F}$) (human), were obtained from Napier et al. (1999) [55]. Receptor occupancies were predicted according to Eq. 16 and plotted against a range of unbound plasma concentrations to obtain full concentration-receptor occupancy profiles [54]. The horizontal dotted lines represent the 50% fractional receptor occupancy levels. The vertical dotted lines represent reported mean therapeutic C_{max} as unbound concentrations of eletriptan and sumatriptan after 40 mg PO or 50 mg/100 mg PO, respectively, in humans [37, 38]. **B** The predicted 5-HT$_{1B}$ receptor occupancy of eletriptan in humans. **C** The predicted 5-HT$_{1D}$ receptor occupancy of eletriptan in humans. **D** The predicted 5-HT$_{1F}$ receptor occupancy of eletriptan in humans **(E)** The predicted 5-HT$_{1B}$ receptor occupancy of sumatriptan in humans. **F** The predicted 5-HT$_{1D}$ receptor occupancy of sumatriptan in humans. **G** The predicted 5-HT$_{1F}$ receptor occupancy of sumatriptan in humans. All predicted receptor occupancies have been fitted to non-linear regression [agonist] vs. response with variable slope (four parameters)

Estimated unbound target-site concentrations were in combination with publicly available 5-HT_{1B}, 5-HT_{1D}, and 5-HT_{1F} receptor affinity constants used to predict therapeutic receptor occupancies in the trigeminal ganglion and in the whole brain according to Eq. 16 [55].

The receptor occupancy estimates as function of unbound plasma concentrations are shown in Fig. 5B-G. The substantial difference in the $K_{p,\ uu}$ between the trigeminal ganglion and the whole brain was found to impact the regional receptor occupancy levels at clinically relevant plasma concentrations. We estimated almost complete 5-$HT_{1B/1D}$ receptor occupancies in the trigeminal ganglion for both eletriptan and sumatriptan, while lower occupancies were estimated in the brain (Table 2). For example, at therapeutic C_{max}, eletriptan was predicted to achieve 84% occupancy of 5-HT_{1B} receptors in the trigeminal ganglion and 37% in the brain. In contrast, the 5-HT_{1F} receptor occupancy for eletriptan was estimated to be considerably lower in both the whole brain and trigeminal ganglion.

Overall, our predictions indicate that both eletriptan and sumatriptan reach unbound concentrations that may be capable of stimulating 5-$HT_{1B/1D/1F}$ receptors, not only in the trigeminal ganglion but also within the CNS at clinically relevant conditions.

Discussion

The ability of triptans to cross the BBB sufficiently to contribute to their antimigraine effects via central 5-$HT_{1B/1D/1F}$ receptors has been debated for decades [8, 9, 23, 27, 28]. Our study sought to clarify this by investigating the regional distribution of unbound eletriptan and sumatriptan in the PNS and CNS. We have shown that despite the low extent of BBB transport, eletriptan and sumatriptan may achieve unbound brain concentrations sufficient to engage with central targets, supporting the likelihood of an additional central site of action.

Heterogenic triptan transport across PNS and CNS barriers with the most pronounced distribution into the trigeminal ganglion

Both eletriptan and sumatriptan demonstrated substantial differences in the extent of transport across the endothelial barriers of the PNS and CNS. The $K_{p,\ uu,\ whole\ brain}$ values were ≤ 0.06 for both drugs indicating predominant active efflux at the BBB. Our findings align well with previously shown $K_{p,\ uu,\ brain}$ values of 0.04 to 0.06 for eletriptan [20, 22, 58] and 0.05 to 0.07 for sumatriptan [58, 59]. Both eletriptan [19–22, 60] and sumatriptan [19, 61] have been identified as substrates of the efflux transporter, P-glycoprotein (P-gp). P-gp interactions may explain the low $K_{p,\ uu}$ values across the BBB and BSCB. The efflux was preserved across all investigated brain regions, yet with extensively varying extents of transport (>6-fold variation) indicating region-specific differences in BBB function. Inter-regional changes might influence the pharmacological potential of triptans depending on which regions are involved. The hypothalamus exhibited the highest brain exposure of both triptans. This increased exposure may be attributed to the median eminence, a circumventricular organ, in the hypothalamus, which might explain the higher $K_{p,\ uu}$ found in this region [62].

We observed the highest drug distribution into the trigeminal ganglion with $K_{p,\ uu,\ TG}$ values of 0.519 and 0.923 for eletriptan and sumatriptan, respectively. These findings indicate that sumatriptan freely penetrates the BNB via passive diffusion or mutually compensated efflux and influx, while eletriptan is subjected to moderate efflux. The higher triptan distribution into PNS regions might be a result of the BNB being less restrictive compared to the BBB, potentially due to a reduced influence of efflux transporters at the BNB [56]. In addition, a recent study demonstrated substantial differences in paracellular transport between the sciatic nerve barrier and the BBB, as indicated by differences in the $K_{p,\ uu}$ of 4 kDa dextran [18]. This supports the notion that the BNB is a less restrictive barrier compared to the BBB.

Predicted receptor occupancies in the CNS and potential clinical implications

Despite limited BBB penetration of eletriptan and sumatriptan leading to low unbound concentrations in CNS regions, our predictions indicate that central targets may still be relevant at therapeutic doses (Table 2). Notably, eletriptan is estimated to reach a 5-HT_{1D} receptor occupancy of 67% in the whole brain at its peak plasma concentration. This relatively high receptor occupancy in the CNS emphasizes the potential clinical implication herein. In contrast, eletriptan is associated with a considerably lower occupancy of 5-HT_{1F} receptors in the whole brain, estimated around 15%.

Using mathematical predictions, Tokuora et al. (2014) suggested that a 5-HT_{1B} receptor occupancy of 32.0-89.4% and a 5-HT_{1D} receptor occupancy of 68.4–96.2% are necessary to reach clinical effects [54]. These estimates were based on unbound plasma concentrations associated with clinical efficacy, however, not accounting for unbound target-site concentrations [54]. Based on our predictions of brain receptor occupancy, eletriptan is likely to achieve the lower threshold proposed by Tokuora et al. for both receptors at its peak plasma concentration following oral administration of 40 mg. In contrast, sumatriptan is expected to reach the minimally required receptor occupancy only for the central 5-HT_{1B} receptors after a 100 mg oral dose (Table 2). While the exact receptor occupancy required for the clinical effects of triptans remains unclear,

some suggest that even lower receptor occupancy levels might be sufficient for the clinical efficacy of sumatriptan [63]. A positron emission tomography (PET) study showed that sumatriptan displaces a 5-HT_{1B} receptor ligand with a mean occupancy rate of 16 ± 5.3% after clinically relevant dosing of 6 mg subcutaneous injection, reflecting a $C_{tot, max}$ of 72 ng/mL, to a patient experiencing migraine [63, 64]. The mean 16% receptor occupancy of 5-HT_{1B} receptors was demonstrated in the seven pain-modulating regions including the dorsolateral and ventrolateral prefrontal cortex, orbitofrontal cortex, anterior cingulate cortex, sensorimotor cortex, insula, and amygdala [63]. In this regard, our estimates of 21–32% central 5-HT_{1B} receptor occupancy in the whole brain for sumatriptan at 30 ng/mL and 53 ng/mL peak plasma concentrations are in line with the PET imaging study of sumatriptan. It is important to note that the frontal and parietal cortices exhibited the lowest extent of BBB transport in healthy rats, and, on average, unbound ISF concentrations in these regions are expected to be approximately two-fold lower than the whole-brain concentrations used for receptor occupancy estimation. Despite this, our estimates indicate that sumatriptan at doses of 100 mg or higher can achieve 15% or greater receptor occupancy of the 5-HT_{1B} receptor in the cortical areas.

Reported CNS-related side effects after triptan administration support the prospect of central receptor engagement [25]. Ferrari et al. (2002) reported placebo-subtracted CNS side effects of 3.7% after peroral administration of 50 mg sumatriptan, while patients receiving 40 mg eletriptan demonstrated placebo-subtracted CNS side effects of 7.5% [25, 26]. The higher incidence of CNS-related side effects after eletriptan administration complies well with the present study indicating that eletriptan is more likely to stimulate central receptors as compared to sumatriptan (Table 2).

Although we have not investigated the antimigraine effect, herein we demonstrate that a central effect exerted by eletriptan and sumatriptan cannot be excluded, despite their poor BBB penetrating properties.

Study limitations – evaluation of the assumptions

Several assumptions underlie the predictions of receptor occupancies in humans based on rat $K_{p, uu}$ and human in vitro affinity values, each carrying potential limitations that must be acknowledged. One key assumption is that $K_{p, uu}$ is concentration independent. To obtain full concentration-receptor occupancy profiles, simulations were performed within the unbound plasma concentration range of 0.1–10,000 nM. Although concentration-dependent changes in $K_{p, uu}$ could theoretically occur upon saturation of transporters, this is unlikely for P-gp substrates [65, 66]. Moreover, the upper concentration range is unlikely to be achieved at therapeutic doses, making this assumption well-founded for therapeutic predictions. Species differences in the BBB are another critical consideration. As noted previously, both eletriptan [19–22, 60] and sumatriptan [19, 61] are substrates of P-gp, an efflux transporter that is expressed in brain microvasculature at higher levels in rats compared to humans. Uchida et al. (2020) reported that the P-gp expression at the BBB is 10-fold greater in rats than in humans [67]. Consequently, the $K_{p, uu, brain}$ of P-gp substrates, such as eletriptan and sumatriptan, may be higher in humans than in rats. Bauer et al. examined (R)-[^{11}C]verapamil, a known P-gp substrate, in the presence of increasing doses of the P-gp inhibitor tariquidar in a PET imaging study. They showed a 4-fold more pronounced response to P-gp inhibition in rats compared to humans [66]. The latter indicates a potential discrepancy between the absolute protein content and its function. Since the quantitative assessment of $K_{p, uu, brain}$ in humans remains to be one of the ground challenges in the BBB field, we are unable to provide accurate estimates of the level of potential underestimation of brain exposure for the investigated triptans.

In addition, we assumed consistent 5-$HT_{1B/1D/1F}$ expression levels across the studied regions. However, conflicting data may weaken this assumption. On one hand, variations in 5-$HT_{1B/1D/1F}$ receptor expression levels across various brain regions have been reported, wherefore our results must be interpreted with caution [13, 15]. Variability in receptor expression could influence the regional receptor occupancies of triptans. On the other hand, Deen et al. (2019) reported that sumatriptan might occupy 5-HT_{1B} receptors uniformly across various brain regions, suggesting that the selection of specific regions for analysis is unlikely to lead to misinterpretation [63].

Some triptans, such as eletriptan, are known to have active metabolites [26]. In the present study, only parent compounds were analyzed. Since metabolites may have a clinical impact, this is a potential limitation of the study.

In conclusion, while these assumptions are well-founded, they introduce uncertainties that must be considered when interpreting the study findings. If assumptions are violated, it is more likely to result in underestimation rather than overestimation, strengthening the hypothesis of the central site of action.

Conclusion

This study provides the first comprehensive evaluation of eletriptan and sumatriptan distribution across various regions of the CNS and PNS, offering insights into triptans' potential target-sites in migraine therapy. The highest triptan exposure was observed in the trigeminal ganglion, which is a well-known antimigraine target-site. In contrast, both eletriptan and sumatriptan displayed limited BBB transport, with notable inter-regional

variations. We predicted almost complete receptor occupancy in the trigeminal ganglion, with markedly lower but still notable occupancies in the brain, regardless of triptan and receptor subtype.

In conclusion, these findings suggest that eletriptan and sumatriptan can engage with central receptors despite limited BBB transport, supporting their potential for both peripheral and central sites of action in migraine therapy. Although eletriptan and sumatriptan may engage with central receptors, the impact of a central action is still uncertain. Further research is needed to explore whether central receptor occupancy contributes to antimigraine effects and/or CNS side effects in patients.

Abbreviations

5-HT_{1B}	5-hydroxytryptamine receptor subtype 1B
5-HT_{1D}	5-hydroxytryptamine receptor subtype 1D
5-HT_{1F}	5-hydroxytryptamine receptor subtype 1F
aECF	Artificial extracerebral fluid
BBB	Blood-brain barrier
BNB	Blood-nerve barrier
BSCB	Blood-spinal cord barrier
$CaCl_2$	Calcium dichloride
CMA	Combinatory mapping approach
C_{max}	Peak plasma concentration
CNS	Central nervous system
$f_{u,brain}$	Fraction unbound in brain
$f_{u,nerve}$	Fraction unbound in nerve
$f_{u,plasma}$	Fraction unbound in plasma
HEPES	N'-2-Hydroxyethylpiperazine-N'-2 ethane sulphonic acid
ICF	Intracellular fluid
ISF	Interstitial fluid
IV	Intravenous
KCl	Potassium chloride
K_d	Equilibrium dissociation constants
KH_2PO_4	Potassium dihydrogen phosphate
K_p	Total tissue-to plasma concentration ratio
$K_{p,uu,cell}$	Intracellular-to-extracellular cell partitioning coefficient
$K_{p,uu}$	Unbound tissue-to-plasma concentration ratio
LLOQ	Lower limit of quantification
$MgSO_4$	magnesium sulfate
MPA	Mobile phase A
MPB	Mobile phase B
NaCl	sodium chloride
NeuroPK	Neuropharmacokinetic
NS	Nervous system
PBS	Phosphate-buffered saline
PET	Positron emission tomography
PNS	Peripheral nervous system
PO	Peroral
QC	Quality control
RO	Receptor occupancy
ROI	Region of interest
Rpm	Rotations per minute
Ss	Steady state
TG	Trigeminal ganglion
ULOQ	Upper limit of detection
UPLC-MS/MS	Ultra-performance liquid chromatography coupled with a tandem mass spectrometry
v:v	Volume: volume
V_{eff}	Effective plasma volume
$V_{protein}$	Brain vascular volume of plasma protein
$V_{u,brain}$	Unbound volume unbound in brain
V_{water}	Brain vascular volume of plasma water
w:v	Weigh: volume
WB	Whole brain

Supplementary Information

The online version contains supplementary material available at https://doi.org/10.1186/s10194-024-01894-0.

Additional file 1: The bioanalytical method parameters and sample preparation details. Tabel S1. The MS/MS parameter employed for the bioanalysis of sumatriptan, sumatriptan-d6 and eletriptan. Table S2. Liquid chromatography conditions used for bioanalysis of eletriptan and sumatriptan

Additional file 2: Time-concentration plasma profiles and endpoint concentration of eletriptan and sumatriptan. Plasma concentrations of eletriptan and sumatriptan after a 4-hour IV infusion in rats. A) Time-concentration profiles of eletriptan and sumatriptan after a 4-hour IV infusion in male rats. Data not showed for females due to a technical error. B) Endpoint plasma concentrations after terminal heart puncture in male and female rats. Each data point or column represents the mean ± SD.

Additional file 3: K_p and $K_{p,uu}$ with linear scale. Assessment of regional K_p and $K_{p,uu}$ for eletriptan and sumatriptan in rats under steady state. A) Total tissue-to-plasma concentration ratio. B) The unbound tissue-to-plasma concentration ratio. Columns represent mean ± SD. The mean value of each column is annotated within each bar. The dotted line represents the line of unity. Values below unity indicate predominant active efflux across the respective barriers. Values are sorted according to descending $K_p/K_{p,uu}$ values for eletriptan.

Additional file 4: Unbound fractions of eletriptan and sumatriptan in plasma. Unbound fractions of eletriptan and sumatriptan in plasma assessed at 200 nM and 400 nM. Each column represents the mean ± SD. Groups were compared using a two-way ANOVA analysis followed by a Tukey's multiple comparison test

Additional file 5: Unbound fractions of eletriptan and sumatriptan in brain and nerve homogenate. Unbound fractions of eletriptan and sumatriptan in brain and sciatic nerve homogenate. Each column represents the mean ± SD.

Acknowledgements
We thank Milda Girdenyté for her invaluable help and expertise in the isolation of the sciatic nerve and spinal cord. Additionally, we express our gratitude to Jessica Dunhall for her efforts and experimental work in the animal facility. Schematic illustrations and graphical abstract were created with Biorender.com.

Authors' contributions
NS, IL, MK, and BB were involved with study conceptualization and participated in the experimental design. NS, FB, and IL conducted experimental work and data treatment. AG and NS developed, validated, and performed sample preparation and bioanalysis. NS drafted the initial version of the manuscript. All authors participated in finalizing the manuscript and approved the final version of the manuscript.

Funding
Open access funding provided by Uppsala University. This project has received funding from the Innovative Medicines Initiative 2 Joint Undertaking (JU) under grant agreement No 807015 (FB, AG, IL, BB). The JU receives support from the European Union's Horizon 2020 research and innovation programme and EFPIA.

Data availability
No datasets were generated or analysed during the current study.

Declarations

Ethics approval and consent to participate
All animal work was conducted in accordance with the national legislations regulating animal experiments in Sweden.

Consent for publication
Not applicable.

Competing interests
The authors declare no competing interests.

Author details
[1]Department of Pharmacy, CNS Drug Delivery and Barrier Modelling group (CNSBM), University of Copenhagen, Copenhagen, Denmark. [2]Department of Pharmacy, Translational Pharmacokinetics/Pharmacodynamics group (tPKPD), Uppsala University, Uppsala, Sweden.

Received: 1 October 2024 Accepted: 22 October 2024
Published online: 30 October 2024

References

1. Ferrari MD, Goadsby PJ, Burstein R, Kurth T, Ayata C, Charles A et al (2022) Migraine. Nat Rev Dis Primers 8(1):2
2. Eigenbrodt AK, Ashina H, Khan S, Diener H-C, Mitsikostas DD, Sinclair AJ et al (2021) Diagnosis and management of migraine in ten steps. Nat Reviews Neurol 17(8):501–514
3. Karlsson WK, Ostinelli EG, Zhuang ZA, Kokoti L, Christensen RH, Al-Khazali HM et al (2024) Comparative effects of drug interventions for the acute management of migraine episodes in adults: systematic review and network meta-analysis. BMJ 386:e080107
4. Davidsson OB, Olofsson IA, Kogelman LJ, Andersen MA, Rostgaard K, Hjalgrim H et al (2021) Twenty-five years of triptans – a nationwide population study. Cephalalgia 41(8):894–904
5. Negro A, Koverech A, Martelletti P (2018) Serotonin receptor agonists in the acute treatment of migraine: a review on their therapeutic potential. J Pain Res 11:515–526
6. Benemei S, Cortese F, Labastida-Ramírez A, Marchese F, Pellesi L, Romoli M et al (2017) Triptans and CGRP blockade – impact on the cranial vasculature. J Headache Pain 18(1):103
7. Cottier KE, Vanderah TW, Largent-Milnes TM (2017) The CNS as a primary target for migraine therapeutics. Curr Top Pharmacol 21:1–16
8. Tfelt-Hansen PC (2010) Does Sumatriptan cross the blood-brain barrier in animals and man? J Headache Pain 11(1):5–12
9. Ahn AH, Basbaum AI (2005) Where do triptans act in the treatment of migraine? Pain 115(1–2):1–4
10. Tepper SJ, Rapoport AM, Sheftell FD (2002) Mechanisms of action of the 5-HT1B/1D receptor agonists. Arch Neurol 59(7):1084–1088
11. Goadsby PJ, Edvinsson L (1993) The trigeminovascular system and migraine: studies characterizing cerebrovascular and neuropeptide changes seen in humans and cats. Ann Neurol 33(1):48–56
12. Varnäs K, Hall H, Bonaventure P, Sedvall G (2001) Autoradiographic mapping of 5-HT1B and 5-HT1D receptors in the post mortem human brain using [3H]GR 125743. Brain Res 915(1):47–57
13. Castro ME, Pascual J, RomÓN T, Del Arco C, Del Olmo E, Pazos A (1997) Differential distribution of [3H]Sumatriptan binding sites (5-HT1B, 5-HT1D and 5-HT1F receptors) in human brain: focus on Brainstem and spinal cord. Neuropharmacology 36(4):535–542
14. Classey JD, Bartsch T, Goadsby PJ (2010) Distribution of 5-HT(1B), 5-HT(1D) and 5-HT(1F) receptor expression in rat trigeminal and dorsal root ganglia neurons: relevance to the selective anti-migraine effect of triptans. Brain Res 1361:76–85
15. Varnäs K, Hurd YL, Hall H (2005) Regional expression of 5-HT1B receptor mRNA in the human brain. Synapse 56(1):21–28
16. Clemow DB, Johnson KW, Hochstetler HM, Ossipov MH, Hake AM, Blumenfeld AM (2020) Lasmiditan mechanism of action – review of a selective 5-HT1F agonist. J Headache Pain 21(1):71
17. Abbott NJ, Patabendige AA, Dolman DE, Yusof SR, Begley DJ (2010) Structure and function of the blood-brain barrier. Neurobiol Dis 37(1):13–25
18. Hu Y, Girdenyté M, Roest L, Liukkonen I, Siskou M, Bällgren F et al (2024) Analysis of the contributing role of drug transport across biological barriers in the development and treatment of chemotherapy-induced peripheral neuropathy. Fluids Barriers CNS 21(1):13
19. Wilt LA, Nguyen D, Roberts AG (2017) Insights into the molecular mechanism of Triptan Transport by P-glycoprotein. J Pharm Sci 106(6):1670–1679
20. Evans DC, O'Connor D, Lake BG, Evers R, Allen C, Hargreaves R (2003) Eletriptan metabolism by human hepatic cyp450 enzymes and transport by human p-glycoprotein. Drug Metab Dispos 31(7):861–9
21. Mahar Doan KM, Humphreys JE, Webster LO, Wring SA, Shampine LJ, Serabjit-Singh CJ et al (2002) Passive permeability and P-glycoprotein-mediated efflux differentiate central nervous system (CNS) and non-CNS marketed drugs. J Pharmacol Exp Ther 303(3):1029–1037
22. Svane N, Pedersen ABV, Rodenberg A, Ozgür B, Saaby L, Bundgaard C et al (2024) The putative proton-coupled organic cation antiporter is involved in uptake of triptans into human brain capillary endothelial cells. Fluids Barriers CNS 21(1):39
23. Messina R, Christensen RH, Cetta I, Ashina M, Filippi M (2023) Imaging the brain and vascular reactions to headache treatments: a systematic review. J Headache Pain 24(1):58
24. Muzzi M, Zecchi R, Ranieri G, Urru M, Tofani L, De Cesaris F et al (2019) Ultra-rapid brain uptake of subcutaneous sumatriptan in the rat: implication for cluster headache treatment. Cephalalgia 40(4):330–336
25. Ferrari MD, Roon KI, Lipton RB, Goadsby PJ (2001) Oral triptans (serotonin 5-HT1B/1D agonists) in acute migraine treatment: a meta-analysis of 53 trials. Lancet 358(9294):1668–1675
26. Dodick DW, Martin V (2004) Triptans and CNS side-effects: pharmacokinetic and metabolic mechanisms. Cephalalgia 24(6):417–424
27. Deen M, Hansen HD, Hougaard A, da Cunha-Bang S, Nørgaard M, Svarer C et al (2018) Low 5-HT1B receptor binding in the migraine brain: a PET study. Cephalalgia 38(3):519–527
28. Kogelman LJA, Falkenberg K, Ottosson F, Ernst M, Russo F, Stentoft-Hansen V et al (2023) Multi-omic analyses of triptan-treated migraine attacks gives insight into molecular mechanisms. Sci Rep 13(1):12395
29. Hammarlund-Udenaes M (2010) Active-site concentrations of chemicals - are they a better predictor of effect than plasma/organ/tissue concentrations? Basic Clin Pharmacol Toxicol 106(3):215–220
30. Loryan I, Sinha V, Mackie C, Van Peer A, Drinkenburg W, Vermeulen A et al (2014) Mechanistic understanding of brain drug disposition to optimize the selection of potential neurotherapeutics in drug discovery. Pharm Res 31(8):2203–2219
31. Loryan I, Melander E, Svensson M, Payan M, Konig F, Jansson B et al (2016) In-depth neuropharmacokinetic analysis of antipsychotics based on a novel approach to estimate unbound target-site concentration in CNS regions: link to spatial receptor occupancy. Mol Psychiatry 21(11):1527–1536
32. Fridén M, Gupta A, Antonsson M, Bredberg U, Hammarlund-Udenaes M (2007) In vitro methods for estimating unbound drug concentrations in the brain interstitial and intracellular fluids. Drug Metab Dispos 35(9):1711–1719
33. Fridén M, Bergström F, Wan H, Rehngren M, Ahlin G, Hammarlund-Udenaes M et al (2011) Measurement of unbound drug exposure in brain: modeling of pH partitioning explains diverging results between the brain slice and brain homogenate methods. Drug Metab Dispos 39(3):353–362
34. Percie du Sert N, Hurst V, Ahluwalia A, Alam S, Avey MT, Baker M et al (2020) The ARRIVE guidelines 2.0: updated guidelines for reporting animal research. BMC Vet Res 16(1):242
35. Hammarlund-Udenaes M, Fridén M, Syvänen S, Gupta A (2008) On the rate and extent of drug delivery to the brain. Pharm Res 25(8):1737–1750
36. Loryan I, Reichel A, Feng B, Bundgaard C, Shaffer C, Kalvass C et al (2022) Unbound brain-to-plasma partition coefficient, kp,uu,brain—a game changing parameter for CNS drug discovery and development. Pharm Res 39(7):1321–1341
37. Ferrari A, Tiraferri I, Neri L, Sternieri E (2011) Why pharmacokinetic differences among oral triptans have little clinical importance: a comment. J Headache Pain 12(1):5–12
38. Kim YK, Shin KH, Alderman J, Yu KS, Jang IJ, Lee S (2018) Pharmacokinetics and tolerability of eletriptan hydrobromide in healthy Korean subjects. Drug Des Devel Ther 12:331–337
39. Fridén M, Ljungqvist H, Middleton B, Bredberg U, Hammarlund-Udenaes M (2009) Improved measurement of drug exposure in the Brain using drug-specific correction for residual blood. J Cereb Blood Flow Metab 30(1):150–161
40. Kalvass JC, Maurer TS (2002) Influence of nonspecific brain and plasma binding on CNS exposure: implications for rational drug discovery. Biopharm Drug Dispos 23(8):327–338

41. Loryan I, Fridén M, Hammarlund-Udenaes M (2013) The brain slice method for studying drug distribution in the CNS. Fluids Barriers CNS 10(1):6
42. Fridén M, Ducrozet F, Middleton B, Antonsson M, Bredberg U, Hammarlund-Udenaes M (2009) Development of a high-throughput brain slice method for studying drug distribution in the central nervous system. Drug Metab Dispos 37(6):1226–1233
43. DrugBank online. Eletriptan DB00216, Sumatriptan DB00669. Available from: https://go.drugbank.com/drugs. Cited 2024, August 23rd.
44. Bebawy LI, Moustafa AA, Abo-Talib NF (2003) Stability-indicating methods for the determination of sumatriptan succinate. J Pharm Biomed Anal 32(6):1123–1133
45. Fish DN, Beall HD, Goodwin SD, Fox JL (1997) Stability of sumatriptan succinate in extemporaneously prepared oral liquids. Am J Health Syst Pharm 54(14):1619–1622
46. Jocić B, Zečević M, Živanović L, Protić A, Jadranin M, Vajs V (2009) Study of forced degradation behavior of Eletriptan hydrobromide by LC and LC–MS and development of stability-indicating method. J Pharm Biomed Anal 50(4):622–629
47. Ponnuru VS, Challa BR, Nadendla R (2011) Quantitative analysis of eletriptan in human plasma by HPLC-MS/MS and its application to pharmacokinetic study. Anal Bioanal Chem 401(8):2539–2548
48. Balaji N, Sivaraman V, Neeraja P (2013) A validated UPLC method for the determination of process-related impurities in Antimigraine bulk drug. J Appl Chem 3:20–28
49. Kumbhar AB, Galgatte UC, Warkad SD, Santhakumari B (eds) (2013) Development and validation of a sensitive bioanalytical method for the determination of sumatriptan in rat plasma BY UPLC-MS. https://api.semanticscholar.org/CorpusID:41612105. https://www.semanticscholar.org/paper/DEVELOPMENT-AND-VALIDATION-OF-A-SENSITIVE-METHOD-OF-Kumbhar-Galgatte/7a6a94785124f20b1ce3ae4f8f6db4ef581bfa5e
50. Udutha S, Shankar G, Borkar RM, Kumar K, Srinivasulu G, Guntuku L et al (2018) Identification and characterization of stress degradation products of sumatriptan succinate by using LC/Q-TOF-ESI-MS/MS and NMR: toxicity evaluation of degradation products. J Mass Spectrom 53(10):963–975
51. Vandelli D, Palazzoli F, Verri P, Rustichelli C, Marchesi F, Ferrari A et al (2016) Development and validation of a liquid chromatography-tandem mass spectrometric assay for quantitative analyses of triptans in hair. J Chromatogr B 1017–1018:136–144
52. Wichitnithad W, Nantaphol S, Vicheantawatchai P, Kiatkumjorn T, Wangkangwan W, Rojsitthisak P (2020) Development and validation of liquid chromatography-tandem mass spectrometry method for simple analysis of sumatriptan and its application in bioequivalence study. Pharmaceuticals 13(2):21
53. FDA (2022) Guidance for industry: bioanalytical method validation and study sample analysis
54. Tokuoka K, Takayanagi R, Suzuki Y, Watanabe M, Kitagawa Y, Yamada Y (2014) Theory-based analysis of clinical efficacy of triptans using receptor occupancy. J Headache Pain 15(1):85
55. Napier C, Stewart M, Melrose H, Hopkins B, McHarg A, Wallis R (1999) Characterisation of the 5-HT receptor binding profile of eletriptan and kinetics of [3H]eletriptan binding at human 5-HT1B and 5-HT1D receptors. Eur J Pharmacol 368(2):259–268
56. Liu H, Chen Y, Huang L, Sun X, Fu T, Wu S et al (2018) Drug distribution into peripheral nerve. J Pharmacol Exp Ther 365(2):336–345
57. Reichel A (2014) Integrated approach to optimizing CNS penetration in drug discovery: from the Old to the new paradigm and assessment of drug–transporter interactions. In: Hammarlund-Udenaes M, de Lange ECM, Thorne RG (eds) Drug delivery to the brain: physiological concepts, methodologies and approaches. Springer New York, New York, NY, pp 339–374
58. Kalvass JC, Maurer TS, Pollack GM (2007) Use of plasma and brain unbound fractions to assess the extent of Brain distribution of 34 drugs: comparison of unbound concentration ratios to in vivo P-Glycoprotein efflux ratios. Drug Metab Dispos 35(4):660–666
59. Culot M, Fabulas-da Costa A, Sevin E, Szorath E, Martinsson S, Renftel M et al (2013) A simple method for assessing free brain/free plasma ratios using an in vitro model of the blood brain barrier. PLoS ONE 8(12):e80634
60. Doan KMM, Humphreys JE, Webster LO, Wring SA, Shampine LJ, Serabjit-Singh CJ et al (2002) Passive permeability and P-Glycoprotein-mediated efflux differentiate Central Nervous System (CNS) and Non-CNS marketed drugs. J Pharmacol Exp Ther 303(3):1029–1037
61. Chen C, Zhou H, Guan C, Zhang H, Li Y, Jiang X et al (2020) Applicability of free drug hypothesis to drugs with good membrane permeability that are not efflux transporter substrates: a microdialysis study in rats. Pharmacol Res Perspect 8(2):e00575
62. Imbernon M, Saponaro C, Helms HCC, Duquenne M, Fernandois D, Deligia E et al (2022) Tanycytes control hypothalamic liraglutide uptake and its anti-obesity actions. Cell Metabol 34(7):1054-63e7
63. Deen M, Hougaard A, Hansen HD, Schain M, Dyssegaard A, Knudsen GM et al (2019) Association between Sumatriptan treatment during a migraine attack and central 5-HT1B receptor binding. JAMA Neurol 76(7):834–840
64. Hargreaves RJ (2000) Pharmacology and potential mechanisms of action of Rizatriptan. Cephalalgia 20(Suppl 1):2–9
65. Bauer M, Karch R, Zeitlinger M, Philippe C, Römermann K, Stanek J et al (2015) Approaching complete inhibition of P-Glycoprotein at the human blood–brain barrier: an (R)-[11 C]Verapamil PET Study. J Cereb Blood Flow Metabolism 35(5):743–746
66. Bauer M, Zeitlinger M, Karch R, Matzneller P, Stanek J, Jäger W et al (2012) Pgp-mediated interaction between (R)-[11 C]verapamil and tariquidar at the human blood-brain barrier: a comparison with rat data. Clin Pharmacol Ther 91(2):227–233
67. Uchida Y, Yagi Y, Takao M, Tano M, Umetsu M, Hirano S et al (2020) Comparison of absolute protein abundances of transporters and receptors among blood-brain barriers at different cerebral regions and the blood-spinal cord barrier in humans and rats. Mol Pharm 17(6):2006–2020

Publisher's Note